

One-loop unquenched three-gluon and ghost-gluon vertices in the Curci-Ferrari model

Felipe Figueroa

Laboratoire d'Annecy-le-Vieux de Physique Théorique LAPTh, Université Savoie Mont Blanc, CNRS, F-74000 Annecy, France

Marcela Peláez

Instituto de Física, Facultad de Ingeniería, Universidad de la República, J.H.y Reissig 565, 11000 Montevideo, Uruguay



(Received 26 October 2021; accepted 6 April 2022; published 10 May 2022)

In this article we study the unquenched three-gluon and ghost-gluon vertex in the entire momentum range from the ultraviolet to infrared regime using the Curci-Ferrari model at one loop in Landau gauge, as an extension of the results presented in by Peláez *et al.* [*Phys. Rev. D* **88**, 125003 (2013)]. Results are compared with recent lattice data for SU(3) in the unquenched case. This calculation is a pure prediction of the model because it does not require fixing any parameter once two-point functions are fitted. An analysis of the influence of dynamical quarks at the position of the zero crossing of the three-gluon vertex is presented. Due to the recent improvements in infrared lattice data for the quenched three-gluon correlation function [*Phys. Lett. B* **818**, 136352 (2021)], we also redo the comparison between our one-loop results in this limit and the lattice results, obtaining a very good match.

DOI: [10.1103/PhysRevD.105.094005](https://doi.org/10.1103/PhysRevD.105.094005)

I. INTRODUCTION

The infrared sector of QCD is usually called the non-perturbative regime due to the fact that standard perturbation theory based on the Faddeev-Popov Lagrangian presents a Landau pole in the infrared. This implies that perturbation theory cannot be applied together with this particular gauge-fixed Lagrangian to study the low-energy region. For these reasons, different semianalytical alternatives have been developed in order to approach this regime, such as approaches using nonperturbative functional techniques as treatments based on the Schwinger-Dyson equations (SD) (see, e.g., Refs. [1–22]), the functional renormalization group [23–29], or the variational Hamiltonian approach [30]. Other approaches focus on the fact that the Faddeev-Popov procedure—generally used to fix the gauge—is not completely justified in the infrared due to the existence of Gribov copies [31]. However, until now, it is not known how to build a gauge-fixing procedure from first principles that properly takes into account the problem of Gribov copies in the infrared. There are some interesting attempts to reach this gauge-fixed Lagrangian based on the

Gribov-Zwanziger action and the refined Gribov-Zwanziger approach [32–34].

On top of these semianalytical studies there are lattice simulations. Lattice simulations can deal with the problem of Gribov copies, so they are a good tool to obtain information about the infrared behavior of Yang-Mills theory. Two important observations of lattice simulations are that the gluon propagator reaches a finite nonzero value in the infrared, thus behaving as a massive-like propagator in this region [35–40], and that the relevant expansion parameter obtained through the ghost-gluon or the three-gluon vertex does not present a Landau pole, and in fact it does not become too large [13,36,41,42]. These points have motivated us to study the infrared regime using a gauge-fixed Lagrangian with a gluon mass term [43,44]. This Lagrangian is a particular case of Curci-Ferrari Lagrangians in Landau gauge (CF) [45]. Apart from this model, lattice results also motivates a other approaches, for instance, a screened massive perturbation theory [46–49].

Even though we do not know how to justify the CF Lagrangian from first principles, it is important to observe that it can reproduce a great variety of correlation functions using the first order in perturbation theory. It is important to mention that we do not attempt to reproduce all infrared quantities of QCD perturbatively. In particular, the perturbative expansion for correlation functions involving quarks within the CF model near the chiral limit fails. Other approaches using the CF model were proposed in

Published by the American Physical Society under the terms of the Creative Commons Attribution 4.0 International license. Further distribution of this work must maintain attribution to the author(s) and the published article's title, journal citation, and DOI. Funded by SCOAP³.

Refs. [50,51] in order to explore the chiral limit. See Ref. [52] for a detailed summary of the already studied properties of the model. In particular, one-loop corrections within the CF model were computed for propagators, the ghost-gluon vertex, and the quenched three-gluon vertex [44,53–56]. In addition, two-loop corrections were studied for propagators [57,58] and the ghost-gluon vertex with a vanishing gluon momentum [59] obtaining very good fittings with lattice data. It is important to mention that vertices are obtained as a pure prediction of the model, in the sense that the free parameters are fixed by minimizing the error between propagators and the corresponding lattice data, and therefore there are no free parameters left when studying vertices.

The aim of this article is to extend the study of one-loop corrections for the three-gluon vertex in the presence of dynamical quarks. The infrared regime of the three-gluon vertex has been studied using different approaches (see, e.g., Refs. [15,28,53,60–80]) as it is an important ingredient to understand QCD at low energies. The three-gluon vertex is more difficult to calculate than the propagators because, instead of depending on a single momentum, it depends on three independent scalars. Moreover, it has a richer tensorial decomposition, so different scalar functions (associated with different tensors) have to be reproduced together.

In this article, we study the one-loop effects of dynamical quarks in the three-gluon vertex using the CF model. The unquenched results are compared with lattice data from Ref. [81]. Moreover, recent simulations of the quenched three-gluon vertex show a better handling of the infrared regime, yielding more precise data in this limit [60]. For this reason, it is worth extending the results presented in Ref. [53] for SU(2) to the SU(3) gauge group and comparing them with the newest lattice data. For both cases—quenched and unquenched—the parameters used in the plots are chosen to minimize the error (understood as discrepancy with the lattice) of the propagators previously computed in Refs. [54,57]. In this sense, the results shown in this article are a pure prediction of the model that reproduces the lattice data with great accuracy. Due to the presence of massless ghosts, the CF model also features a zero crossing, as observed in Refs. [18,28,53,60,65–76]. We also find that the inclusion of dynamical quarks shifts the zero crossing towards the infrared in a way consistent with that observed in Refs. [68,69].

The article is organized as follows. In Sec. II we describe the Curci-Ferrari model in Landau gauge in more detail. We give some details on the one-loop calculations of the three-gluon vertex in Sec. III in terms of the Ball-Chiu components. In Sec. IV we present the renormalization conditions and renormalization group

equations. We present our results in Sec. V and compare them with lattice data. At the end of the article we present our conclusions.

II. CURCI-FERRARI MODEL WITH QUARKS

We start by introducing the Curci-Ferrari Lagrangian [45] in the presence of dynamical quarks in Euclidean space:

$$\mathcal{L} = \frac{1}{4}(F_{\mu\nu}^a)^2 + \partial_\mu \bar{c}^a (D_\mu c)^a + ih^a \partial_\mu A_\mu^a + \frac{m^2}{2}(A_\mu^a)^2 + \sum_{i=1}^{N_f} \bar{\psi}_i (\gamma_\mu D_\mu + M_i) \psi_i, \quad (1)$$

where g is the coupling constant, and the flavor index i spans the N_f quark flavors.

The covariant derivative D_μ acting on a ghost field in the adjoint representation of SU(N) reads $(D_\mu c)^a = \partial_\mu c^a + gf^{abc} A_\mu^b c^c$, while when applied to a quark in the fundamental representation it reads $D_\mu \psi = \partial_\mu \psi - gt^a A_\mu^a \psi$. The latin indices correspond to the SU(N) gauge group, the t^a are the generators in the fundamental representation, and the f^{abc} are the structure constants of the group. Finally, the field strength is given by $F_{\mu\nu}^a = \partial_\mu A_\nu^a - \partial_\nu A_\mu^a + gf^{abc} A_\mu^b A_\nu^c$.

The Feynman rules associated with this Lagrangian are the standard Feynman rules for Euclidean QCD in Landau gauge except for the gluon's free propagator, which reads

$$\langle A_\mu^a A_\nu^b \rangle_0(p) = \delta^{ab} P_{\mu\nu}^\perp(p) \frac{1}{p^2 + m^2}, \quad (2)$$

where we have introduced the transverse projector

$$P_{\mu\nu}^\perp(p) = \delta_{\mu\nu} - \frac{p_\mu p_\nu}{p^2}. \quad (3)$$

It is important to mention that the gluon mass term added to the Faddeev-Popov Lagrangian breaks the BRST symmetry. However, it can be shown that Eq. (1) satisfies a modified (non-nilpotent) BRST symmetry that can be used to prove its renormalizability [82].

Probably the most interesting aspect of this model is the fact that, as has been shown in various previous articles (see, e.g., Refs. [43,44,56,57,83]), the addition of a gluon mass term regularizes the theory in the infrared, allowing for a perturbative treatment of the theory in this region. More specifically, it is possible to find a renormalization scheme without an infrared Landau pole for particular choices of the initial condition of the renormalization-group flow. These features have made it possible to use this model to compute various two- and three-point

functions to one- and two-loop orders, obtaining a very good match with lattice simulations [44,53–55,57–59]. It is important to mention that this model has also been studied at finite temperature and chemical potential in Refs. [84–86].

III. ONE-LOOP CALCULATION OF THE THREE-GLUON VERTEX

A. Tensorial structure and computation

In this work we extend the one-loop computation of the gluon three-point function obtained in Ref. [53] for $SU(N)$ Yang-Mills theory to unquenched QCD. In order to calculate the gluon's three-point function at one-loop order we need to compute the Feynman diagrams shown in Fig. 1.

As shown in Ref. [87], the color structure of the three-gluon vertex is simply the structure constant f^{abc} of the $SU(N)$ group, so it can be factored out. Furthermore, we follow the usual convention [88] of factorizing the coupling constant, and thus we define

$$\Gamma_{A_\mu^a A_\nu^b A_\rho^c}^{(3)}(p, k, r) = -igf^{abc}\Gamma_{\mu\nu\rho}(p, k, r).$$

The tensor structure of $\Gamma_{\mu\nu\rho}(p, k, r)$ can be easily deduced: it must depend on three Lorentz indices (one for each gluon) and two independent momenta due to momentum conservation. As a consequence, we can have only two types of tensor structures: those made up of three momenta ($p_\mu p_\nu p_\rho, p_\mu p_\nu k_\rho, \dots$), and those made up of one momentum and the Euclidean metric tensor ($p_\mu \delta_{\nu\rho}, k_\nu \delta_{\mu\rho}, \dots$). It is not hard to convince oneself that there are eight possible

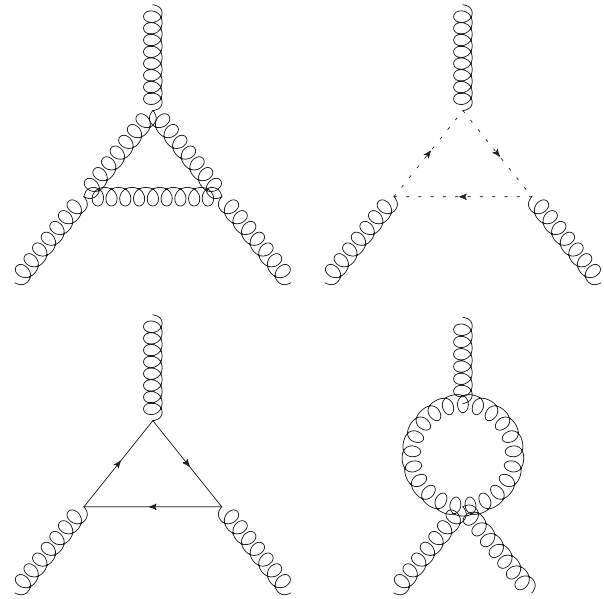


FIG. 1. Feynman diagrams present in the one-loop calculation of the three-gluon vertex.

terms of the first kind and six of the second, adding up to a total of 14 possible terms in the vertex's tensor structure. However, the vertex is symmetric under the exchange of any pair of external legs, and this ends up reducing the total number of possible independent coefficients in the vertex's tensor structure to six.

A cleaner way of exploiting these symmetries is by following the decomposition proposed by Ball and Chiu in Ref. [89], where they parametrized the vertex using six scalar functions:

$$\begin{aligned} \Gamma_{\mu\nu\rho}(p, k, r) = & A(p^2, k^2, r^2)\delta_{\mu\nu}(p-k)_\rho + B(p^2, k^2, r^2)\delta_{\mu\nu}(p+k)_\rho - C(p^2, k^2, r^2)(\delta_{\mu\nu}p \cdot k - p_\nu k_\mu)(p-k)_\rho \\ & + \frac{1}{3}S(p^2, k^2, r^2)(p_\rho k_\mu r_\nu + p_\nu k_\rho r_\mu) + F(p^2, k^2, r^2)(\delta_{\mu\nu}p \cdot k - p_\nu k_\mu)(p_\rho k_r - k_\rho p_r) \\ & + H(p^2, k^2, r^2) \left[-\delta_{\mu\nu}(p_\rho k_r - k_\rho p_r) + \frac{1}{3}(p_\rho k_\mu r_\nu - p_\nu k_\rho r_\mu) \right] + \text{cyclic permutations.} \end{aligned} \quad (4)$$

The scalar functions have the following symmetry properties: A , C , and F are symmetric under permutation of the first two arguments; B is antisymmetric under permutation of the first two arguments; H is completely symmetric and S is completely antisymmetric.

It is important to note that only some of these scalar functions are accessible through lattice simulations, since they have access to the vertex function only through the correlation function, i.e., the vertex contracted with the full external propagators. Since the propagators in Landau gauge are transverse, the longitudinal part of the vertex

function is lost in the process when requiring the conservation of momentum at the vertex. In particular, this means that the B and S functions are not accessible through lattice computations.

We decompose every diagram contributing to the three-gluon vertex into the Ball-Chiu tensorial structure. In this way, we obtain the contribution of each diagram to each of the scalar functions A , B , C , F , H , and S . To perform our computations, we express the integrals in the Feynman diagrams of Fig. 1 in terms of only three master integrals (defined following the convention in Ref. [90]) as

$$\begin{aligned}
\mathbf{A}[m_1] &= \bar{C} \int d^d q \frac{1}{[q^2 + m_1^2]}, \\
\mathbf{B}[p_1, m_1, m_2] &= \bar{C} \int d^d q \frac{1}{[q^2 + m_1^2][(q + p_1)^2 + m_2^2]}, \\
\mathbf{C}[p_1, p_2, m_1, m_2, m_3] &= \bar{C} \int d^d q \frac{1}{[q^2 + m_1^2][(q + p_1)^2 + m_2^2][(q - p_2)^2 + m_3^2]},
\end{aligned} \tag{5}$$

where $\bar{C} = 16\pi^2 \frac{\bar{\mu}^{2\epsilon}}{(2\pi)^d}$, and the regularization scale $\bar{\mu}$ is related to the renormalization scale μ by $\mu^2 = 4\pi e^{-\gamma} \bar{\mu}^2$. The \mathbf{A} and \mathbf{B} master integrals can be solved analytically in $d = 4 - 2\epsilon$ in terms of the external momentum and the masses, but the \mathbf{C} master integral must be treated numerically except for particular kinematics. We chose the FIRE5 algorithm [91] to perform the master integral reduction, thus obtaining analytic expressions for each of the scalar functions in terms of the three master integrals for arbitrary momentum configurations. The expressions are complicated and not very enlightening; however, the explicit expressions appear in the supplemental material of Ref. [53] for the quenched case, while the quark contribution can be found in Ref. [88]. In the case of one vanishing external momentum, the computation becomes much simpler and the result for the quenched vertex function in this configuration was given in Ref. [53], while the unquenched case is presented in the Appendix.

B. Checks

Yang-Mills results were already checked in Ref. [53]. We only need to check the quark triangle diagram to test our unquenched results. To do this, we compare our results to those of Ref. [88], verifying that they yield the same expressions when properly transformed to Euclidean space. This is expected, as the quark triangle diagram is independent of the mass of the gluons and therefore its contribution in the Curci-Ferrari model is the same as in standard QCD.

IV. RENORMALIZATION AND RENORMALIZATION GROUP

In this section, we introduce the renormalization scheme that we use in this work and explain how we implement renormalization-group ideas to improve our perturbative calculation.

A. Renormalization

To take care of the divergences appearing in the one-loop quantities, we take the usual approach of redefining the fields, masses, and coupling constants through renormalization factors that absorb the infinities. The renormalized quantities are defined in terms of the bare ones (denoted with a “0” subscript) as follows:

$$\begin{aligned}
A_0^{a\mu} &= \sqrt{Z_A} A^{a\mu}, & \psi_0 &= \sqrt{Z_\psi} \psi, \\
c_0^a &= \sqrt{Z_c} c^a, & \bar{c}_0^a &= \sqrt{Z_c} \bar{c}^a, \\
g_0 &= Z_g g, & m_0^2 &= Z_m m^2, & M_0 &= Z_M M.
\end{aligned} \tag{6}$$

From now on, all expressions will refer to renormalized quantities unless explicitly stated otherwise. The renormalized propagators and the three-gluon one-particle-irreducible correlation function are thus defined as

$$\begin{aligned}
\Gamma_{A_\mu^a A_\nu^b}^{(2)}(p) &= Z_A \Gamma_{A_\mu^a A_\nu^b, 0}^{(2)}(p), \\
\Gamma_{c^a \bar{c}^b}^{(2)}(p) &= Z_c \Gamma_{c^a \bar{c}^b, 0}^{(2)}(p), \\
\Gamma_{\psi \bar{\psi}}^{(2)}(p) &= Z_\psi \Gamma_{\psi \bar{\psi}, 0}^{(2)}(p), \\
\Gamma_{A_\mu^a A_\nu^b A_\rho^c}^{(3)}(p, r) &= Z_A^{3/2} \Gamma_{A_\mu^a A_\nu^b A_\rho^c, 0}^{(3)}(p, r).
\end{aligned} \tag{7}$$

B. Infrared-safe renormalization scheme

To fix the renormalization factors we use the infrared-safe (IS) renormalization scheme defined in Ref. [44]. It is based on a nonrenormalization theorem for the gluon mass [92–94] and is defined by

$$\Gamma^\perp(p = \mu) = m^2 + \mu^2, \quad J(p = \mu) = 1, \quad Z_m^2 Z_A Z_c = 1, \tag{8}$$

where $\Gamma^\perp(p)$ is the transversal part of $\Gamma_{A_\mu^a A_\nu^b}^{(2)}(p)$ and $J(p)$ is the ghost dressing function. To fix the renormalization of the coupling constant we use the Taylor scheme, in which the coupling constant is defined as the ghost-gluon vertex with a vanishing ghost momentum. Requiring that the renormalized vertex is finite leads to a relation among the renormalization factors Z_A , Z_c , and Z_g :

$$Z_g \sqrt{Z_A} Z_c = 1. \tag{9}$$

The divergent part of the renormalization factors for the quenched case were presented in Ref. [44]. Here we show the extension to the unquenched Curci-Ferrari model already computed in Ref. [54,95]. In $d = 4 - 2\epsilon$ they read

$$\begin{aligned}
Z_c &= 1 + \frac{3g^2 N}{64\pi^2 \epsilon}, \\
Z_A &= 1 + \frac{g^2 (13N - 8N_f T_f)}{96\pi^2 \epsilon}, \\
Z_{m^2} &= 1 - \frac{g^2 (35N - 16N_f T_f)}{192\pi^2 \epsilon}, \\
Z_g &= 1 - \frac{g^2 (11N - 4N_f T_f)}{96\pi^2 \epsilon}. \quad (10)
\end{aligned}$$

Finally, the quantity we are interested in is actually $\Gamma_{\mu\nu\rho}$ as defined earlier. Since in its definition we factorized a factor of g , the relation between the renormalized and bare quantities is

$$\Gamma_{\mu\nu\rho}(p, r) = Z_A^{3/2} Z_g \Gamma_{\mu\nu\rho,0}(p, r) = \frac{Z_A}{Z_c} \Gamma_{\mu\nu\rho,0}(p, r),$$

where in the last equality we used Eq. (9).

C. Renormalization group

After the renormalization procedure we obtain a finite expression for the three-gluon vertex, but it comes with the usual loop corrections of the form $\log(\frac{p}{\mu})$. To handle this situation, we implement the renormalization-group flow to take care of the large logarithms coming from loop corrections. First, we define the β functions and anomalous dimensions of the fields:

$$\beta_\chi(g, m^2, \{M_i\}) = \mu \left. \frac{d\chi}{d\mu} \right|_{g_0, m_0^2, M_{i,0}}, \quad (11)$$

$$\gamma_\phi(g, m^2, \{M_i\}) = \mu \left. \frac{d \log Z_\phi}{d\mu} \right|_{g_0, m_0^2, M_{i,0}}, \quad (12)$$

where χ can take the role of the coupling constant, gluon mass, or quark mass, and ϕ represents the different fields A, c, ψ .

The renormalization-group equation for the vertex function with n_A gluon legs and n_c ghost legs reads

$$\left(\mu \partial_\mu - \frac{1}{2} (n_A \gamma_A + n_c \gamma_c) + \beta_g \partial_g + \beta_{m^2} \partial_{m^2} \right) \Gamma^{(n_A, n_c)} = 0. \quad (13)$$

This equation allows us to obtain a relation for the vertex function renormalized at the scale μ_0 and the same vertex function renormalized at a different scale μ :

$$\begin{aligned}
&\Gamma^{(n_A, n_c)}(\{p_i\}; \mu, g(\mu), m^2(\mu), M(\mu)) \\
&= z_A(\mu)^{n_A/2} z_c(\mu)^{n_c/2} \times \Gamma^{(n_A, n_c)}(\{p_i\}; \mu_0, \\
&g(\mu_0), m^2(\mu_0), M(\mu_0)), \quad (14)
\end{aligned}$$

where $g(\mu)$, $m^2(\mu)$, and $M(\mu)$ are obtained by integration of the β functions with initial conditions given at some scale μ_0 , and z_A and z_c are obtained, respectively, from

$$\begin{aligned}
\log z_A(\mu, \mu_0) &= \int_{\mu_0}^{\mu} \frac{d\mu'}{\mu'} \gamma_A(g(\mu'), m^2(\mu')), \\
\log z_c(\mu, \mu_0) &= \int_{\mu_0}^{\mu} \frac{d\mu'}{\mu'} \gamma_c(g(\mu'), m^2(\mu')). \quad (15)
\end{aligned}$$

We can then use the nonrenormalization theorems of Eqs. (8) and (9) to relate the anomalous dimensions and the β functions. It is simple to check that one obtains the following relations:

$$\gamma_A(g, m^2) = 2 \left(\frac{\beta_{m^2}}{m^2} - \frac{\beta_g}{g} \right), \quad (16)$$

$$\gamma_c(g, m^2) = \frac{2\beta_g}{g} - \frac{\beta_{m^2}}{m^2}. \quad (17)$$

Finally, we use these relations to integrate Eq. (15), obtaining analytical expressions for z_A and z_c in terms of the running gluon mass and coupling constant, which is another advantage of the infrared-safe scheme:

$$\begin{aligned}
z_A(\mu, \mu_0) &= \frac{m^4(\mu) g^2(\mu_0)}{m^4(\mu_0) g^2(\mu)}, \\
z_c(\mu, \mu_0) &= \frac{m^2(\mu_0) g^2(\mu)}{m^2(\mu) g^2(\mu_0)}. \quad (18)
\end{aligned}$$

We are now able to express the three-gluon vertex renormalized at the scale μ_0 in terms of the same quantity using a running scale $\mu = p$, thus avoiding the large-logarithms problem. Taking into account the factor of g in the definition of $\Gamma_{\mu\nu\rho}(p, r)$, this reads

$$\Gamma_{\mu\nu\rho}(p, r; \mu_0) = \frac{g^4(p) m^6(\mu_0)}{g^4(\mu_0) m^6(p)} \Gamma_{\mu\nu\rho}(p, r; \mu = p). \quad (19)$$

V. RESULTS

We now present our results for the different scalar functions associated with the three-gluon vertex introduced in the previous section. All of our results correspond to four dimensions and the SU(3) gauge group, and we evaluate the scalar functions in different momentum configurations in order to compare them with the available lattice data.

A. Fixing parameters

The only fitting parameters we need to adjust to compare our results with the lattice data are the overall normalization constant of the gluon three-point function and the initial conditions of the renormalization-group flow,

TABLE I. Values of the masses of the quark and gluon (M_0 and m_0 , respectively) and the coupling constant (g_0) at the renormalization scale $\mu_0 = 1$ GeV obtained by adjusting the two-point functions to lattice data, both for the quenched and unquenched cases with two degenerate quark flavors.

	m_0 (GeV)	M_0 (GeV)	g_0
Quenched	0.35	...	3.6
Unquenched ($N_f = 2$)	0.42	0.13	4.5

i.e., the values of the mass of the gluon, the mass of the quark, and the coupling constant at some renormalization scale μ_0 .

The initial conditions for the renormalization group are best obtained by looking for the set of parameters (m_0 , M_0 , g_0) that produce the best fit between the gluon and ghost propagators computed using the Curci-Ferrari approach and the lattice data, since the lattice results are much more precise for propagators than for three-point functions. This task was done in Refs. [53,57] for different gauge groups and renormalization schemes in the quenched case, and in Ref. [54] including dynamical quarks. For the SU(3) group and the IS scheme, the initial conditions we obtain for the renormalization-group flow at $\mu_0 = 1$ GeV are listed in Table I.

In this work we use these values to compute the one-loop three-gluon vertex, which means that up to the overall normalization constant our results are a pure prediction of the model.

B. Comparison with lattice data

In order to compare with lattice data, we must choose specific momentum configurations for $\Gamma_{\mu\nu\rho}(p_1, p_2, p_3)$. Most available lattice data employs some of the following configurations: the *symmetric configuration*, with $p_1^2 = p_2^2 = p_3^2 = p^2$ and $p_1 \cdot p_2 = p_1 \cdot p_3 = p_2 \cdot p_3 = -\frac{p^2}{2}$; the *asymmetric configuration*, with $p_1 = 0$ and $p_2 = -p_3 = p$; and the *orthogonal configuration*, with $p_1 \cdot p_2 = 0$, $p_1^2 = p_2^2 = p^2$ and $p_3^2 = 2p^2$.

For the quenched case, we compare our results with the lattice data from Ref. [60]. Following their definitions, in the symmetric configuration we work with the scalar functions $\bar{\Gamma}_1^{\text{sym}}$ and $\bar{\Gamma}_2^{\text{sym}}$:

$$g\Gamma_{\mu\nu\rho}(p_1, p_2, p_3) = \bar{\Gamma}_1^{\text{sym}}(s^2)\lambda_1^{\mu\nu\rho}(p_1, p_2, p_3) + \bar{\Gamma}_2^{\text{sym}}(s^2)\lambda_2^{\mu\nu\rho}(p_1, p_2, p_3), \quad (20)$$

where

$$\lambda_1^{\mu\nu\rho}(p_1, p_2, p_3) = \Gamma_{\mu'\nu'\rho'}^{(0)}(p_1, p_2, p_3)P_{\mu'\mu}^\perp(p_1) \times P_{\nu'\nu}^\perp(p_2)P_{\rho'\rho}^\perp(p_3),$$

with $\Gamma_{\mu'\nu'\rho'}^{(0)}(p_1, p_2, p_3)$ defined as the perturbative tree-level tensor of the three-gluon vertex, and $\lambda_2^{\mu\nu\rho}(p_1, p_2, p_3) = \frac{(p_1-p_2)_\rho(p_2-p_3)_\mu(p_3-p_1)_\nu}{p^2}$.

On the other hand, the asymmetric configuration of the vertex is parametrized by a single scalar function $\bar{\Gamma}_3^{\text{asym}}$, defined by

$$g\Gamma_{\mu\nu\rho}(p, -p, 0) = \bar{\Gamma}_3^{\text{asym}}(p^2)\lambda_3^{\mu\nu\rho}(p, -p, 0), \quad (21)$$

with

$$\lambda_3^{\mu\nu\rho}(p, -p, 0) = 2p^\rho P^{\perp\mu\nu}(p). \quad (22)$$

We compare our unquenched results with the lattice data from Ref. [81]. They worked in the orthogonal configuration, and defined the usual scalar function G_1 , which consists in contracting the external legs of the vertex with transverse propagators and the tree-level momentum structure of the three-gluon vertex, normalized to the same expression at tree level. This reads

$$G_1(p, k, r) = \frac{\Gamma_{\alpha\beta\gamma}^{\text{tree-level}}(p, k, r)P_{\alpha\mu}^\perp(p)P_{\beta\nu}^\perp(k)P_{\gamma\rho}^\perp(r)\Gamma_{\mu\nu\rho}(p, k, r)}{\Gamma_{\alpha\beta\gamma}^{\text{tree-level}}(p, k, r)P_{\alpha\mu}^\perp(p)P_{\beta\nu}^\perp(k)P_{\gamma\rho}^\perp(r)\Gamma_{\mu\nu\rho}^{\text{tree-level}}(p, k, r)}. \quad (23)$$

The results of the model are shown below using the different scalar functions defined in this section, including the renormalization-group effects.

C. SU(3) Yang-Mills results

We first present our results for SU(3) Yang-Mills theory and compare them with lattice results from Ref. [60]. As stated before, we integrate the beta functions with initial conditions at $\mu_0 = 1$ GeV using the initial conditions listed in Table I.

In Fig. 2 we show the results for the scalar function $\bar{\Gamma}_3^{\text{asym}}$ in the asymmetric configuration (one vanishing momentum), and in Fig. 3 we do the same for the functions $\bar{\Gamma}_1^{\text{sym}}$ and $\bar{\Gamma}_2^{\text{sym}}$ in the symmetric configuration (all momenta equal).

In all cases the agreement is very good, especially considering that the initial conditions for the renormalization-group flow were not fitted for the three-point function, but rather for the propagators. It is also noticeable that in all cases the different scalar functions become negative at low energies, a qualitative feature that was observed in several studies [65,71,73–76]. While the scalar functions associated with the tree-level tensor diverge logarithmically, $\bar{\Gamma}_2^{\text{sym}}$ goes to a constant value in the infrared, as stated in Ref. [60]. The simplicity of the one-loop CF model allows to write the infrared behavior of $\bar{\Gamma}_2^{\text{sym}}$ analytically,

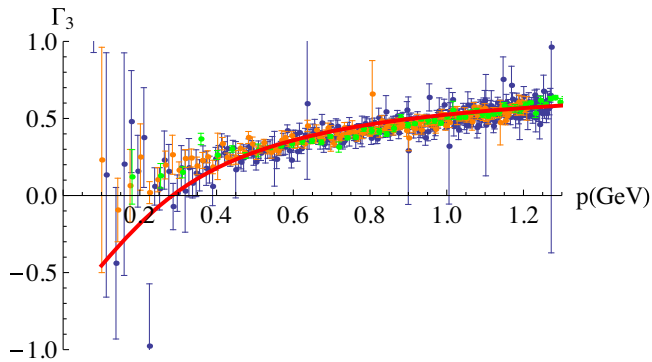


FIG. 2. $\bar{\Gamma}_3^{\text{asym}}$ as a function of momentum for one vanishing momentum (asymmetric configuration). The points are lattice data from Ref. [60]. The plain red line corresponds to our one-loop computation.

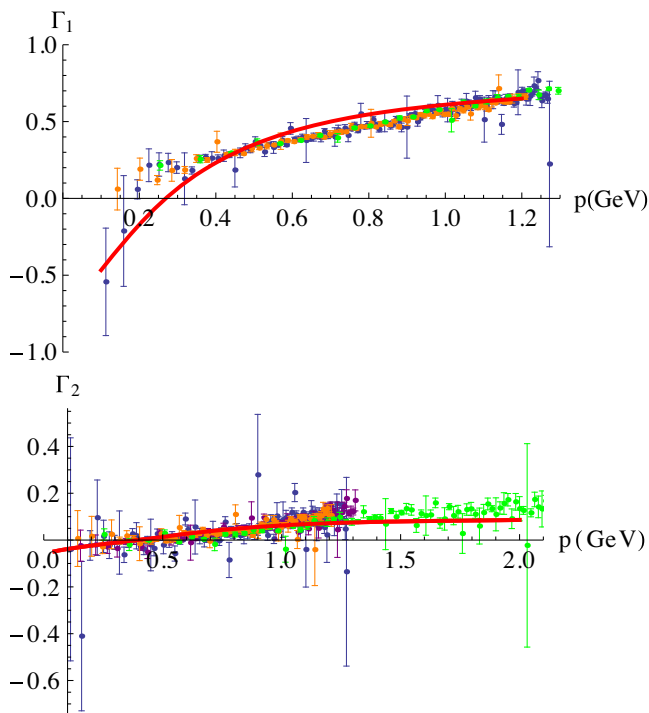


FIG. 3. $\bar{\Gamma}_1^{\text{sym}}$ (top) and $\bar{\Gamma}_2^{\text{sym}}$ (bottom) as a function of momentum in the symmetric configuration. The points are lattice data from Ref. [60]. The plain red line corresponds to our one-loop computation.

$$\bar{\Gamma}_2^{\text{sym}} \sim \frac{g^2 N}{414720\pi^2} \left(20 \left(16\sqrt{3}\text{Cl}_2\left(\frac{\pi}{3}\right) - 33 \right) + 189 \frac{p^2}{m^2} \right), \quad (24)$$

which is indeed finite in the infrared, and where Cl_2 is the Clausen function satisfying $\text{Cl}_2(\frac{\pi}{3}) = 1.0149417$. It is worth mentioning that this behavior is not modified by the effects of the renormalization group.

These results also show the divergent behavior of $\bar{\Gamma}_1$, which can be easily understood due to the presence of massless ghosts, as stated in Ref. [53].

D. Unquenched QCD results

If we want to include the influence of dynamical quarks in the previous computation, we must add the quark triangle diagram to the vertex and use the running of the coupling obtained in the unquenched analysis [54]. The contribution of that diagram can be computed with no difficulty in arbitrary dimension and for an arbitrary number of quarks. Our explicit expressions match those presented in Ref. [88] when continuing them to Euclidean space. In order to be more specific, we show as an example the explicit bare contribution of the quark-loop diagram to the factor G_1 in $d = 4 - 2\epsilon$ dimensions in the Appendix.

The total result for G_1 is shown in Fig. 4 where it is compared with lattice data from Ref. [81]. The data available corresponds to the G_1 scalar function in the case of two mass-degenerate quark flavors ($N_f = 2$) in the orthogonal configuration (two momenta orthogonal to each other and of equal magnitude).

In this case, the agreement is still very good in the infrared but worsens in the UV. More precisely, the model and the lattice results start to separate at a scale of about 2.5 GeV. This scale is of the order of magnitude of the inverse of the lattice spacing used in most lattice simulations, and therefore lattice results beyond this scale are subject to hypercubic lattice-spacing artifacts. Taking this fact into account and also considering that perturbation theory must work at one loop in the UV, we suspect that the decrease in the values of G_1 after the inverse lattice-spacing scale must be caused by finite lattice artifacts.

To confirm this statement, we analytically compute the high-energy limit of G_1 , and find that it behaves in the UV

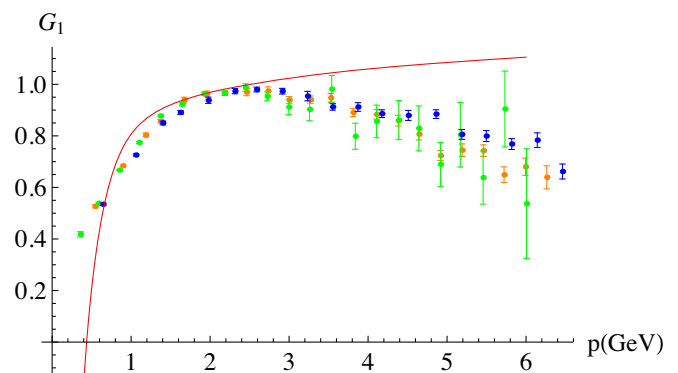


FIG. 4. G_1 scalar function as a function of momentum for two orthogonal momenta (orthogonal configuration) and two mass-degenerate quark flavors. The points are lattice data from Ref. [81]. The plain red line corresponds to our one-loop computation.

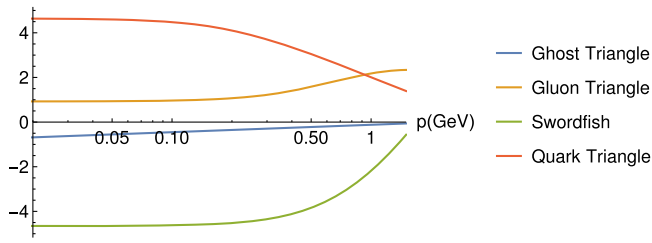


FIG. 5. Infrared behavior of one-loop diagrams contributing to the three-gluon vertex on a logarithmic scale. The ghost triangle contribution goes as $\log p$ in the IR, while the other Feynman diagrams go to a finite value.

as $\text{Ln}(\frac{p}{\mu_0})^\alpha$ with $\alpha = \frac{17N-16N_f T_f}{44N-16N_f T_f}$, which is compatible with our results. The idea behind this computation is that since the UV limit of $G_1(p, p)$ is equal to 1, the high-energy behavior of $G_1(\mu_0, p)$ must be given by $z_A^{-\frac{3}{2}}$ as a consequence of the renormalization-group equation given in Eq. (13). The full computation shows that the UV limit of $z_A^{-\frac{3}{2}}$ is indeed $z_A^{-\frac{3}{2}} \propto \text{Ln}(\frac{\mu}{\mu_0})^{\frac{35}{16}}$ for $N = 3$ and $N_f = 2$. In conclusion, our one-loop computation matches the lattice results in their regime of validity and the renormalization-group prediction in the UV.

To complete the analysis we include the contributions to the three-gluon vertex arising from the different one-loop Feynman diagrams, which are shown in the asymmetric configuration in Fig. 5. Our results match the behavior observed in Ref. [16] for the Yang-Mills contributions, and indeed show that the divergence of the vertex in the infrared is caused by the ghost triangle's logarithmic divergence.

1. Zero crossing and the number of flavors

In this section we study the influence of dynamical quarks at the position of the zero crossing of the three-gluon vertex. In the one-loop CF model the influence of quarks at the renormalized vertex can be isolated as the term proportional to N_f . At one loop, the quarks' contribution to the renormalized vertex is proportional to

$$\mathcal{F} = \left(\frac{3}{2} \delta Z_A^{UQ} \Big|_{\text{finite}} - \delta Z_g^{UQ} \Big|_{\text{finite}} + G_1^{UQ} \Big|_{\text{finite}} \right),$$

where $\delta Z_A^{UQ} \Big|_{\text{finite}}$, $\delta Z_g^{UQ} \Big|_{\text{finite}}$, and $G_1^{UQ} \Big|_{\text{finite}}$ represent the finite parts of the coefficient proportional to $g^2 N_f T_f$ in the Z_A and Z_g renormalization factor and in G_1 , respectively.

We study the sign of the factor \mathcal{F} in order to analyze in which direction the zero crossing is shifted. As \mathcal{F} depends on the finite part of the renormalization factor, it is expected that its sign depends on the chosen renormalization scheme. For the IS scheme we observe that even though the contribution of the quark triangle diagram is positive

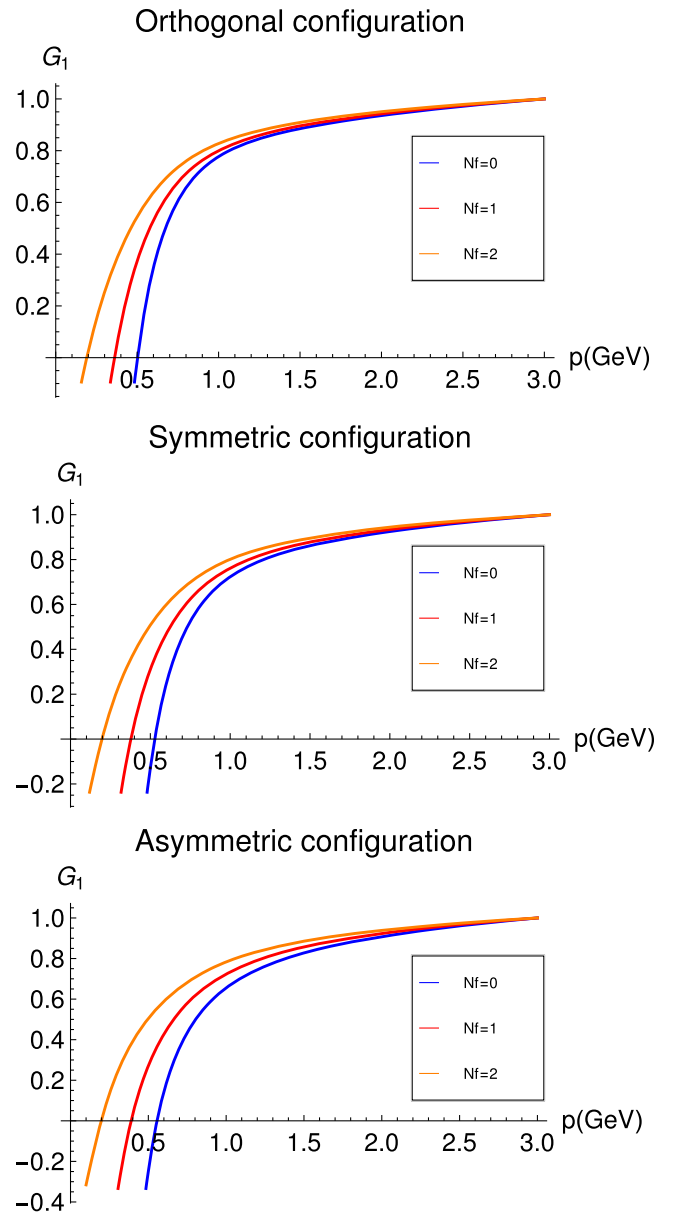


FIG. 6. Comparison of the three-gluon vertex for different values of N_f in the orthogonal configuration (top), symmetric configuration (middle), and gluon vanishing momentum configuration (bottom).

(see Fig. 5), the renormalization factors together with the renormalization-group flow make \mathcal{F} negative. This means that the whole contribution arising from considering dynamical quarks is negative when compared to the quenched quantity using the same flow. However, as flows should be different in each situation, it is better to study the influence of dynamical quarks in the infrared region using the same set of initial conditions of the renormalization group flow at an ultraviolet scale (for instance, $\mu = 3$ GeV). In this context, we can see in Fig. 6 that dynamical quarks shift the zero crossing to the infrared, as was observed in Refs. [68,69].

2. Unquenching the ghost-gluon vertex

It is also interesting to observe the influence of dynamical quarks on the ghost-gluon vertex. Even though quarks do not contribute directly in its one-loop diagrams, the inclusion of dynamical quarks affects its renormalization-group flow.

The function $G^{c\bar{c}A}(p, k, r)$, defined through the vertex as

$$G^{c\bar{c}A}(p, k, r) = \frac{k_\nu P_{\mu\nu}^\perp(r) \Gamma_\mu(p, k, r)}{k_\nu P_{\mu\nu}^\perp(r) k_\mu}, \quad (25)$$

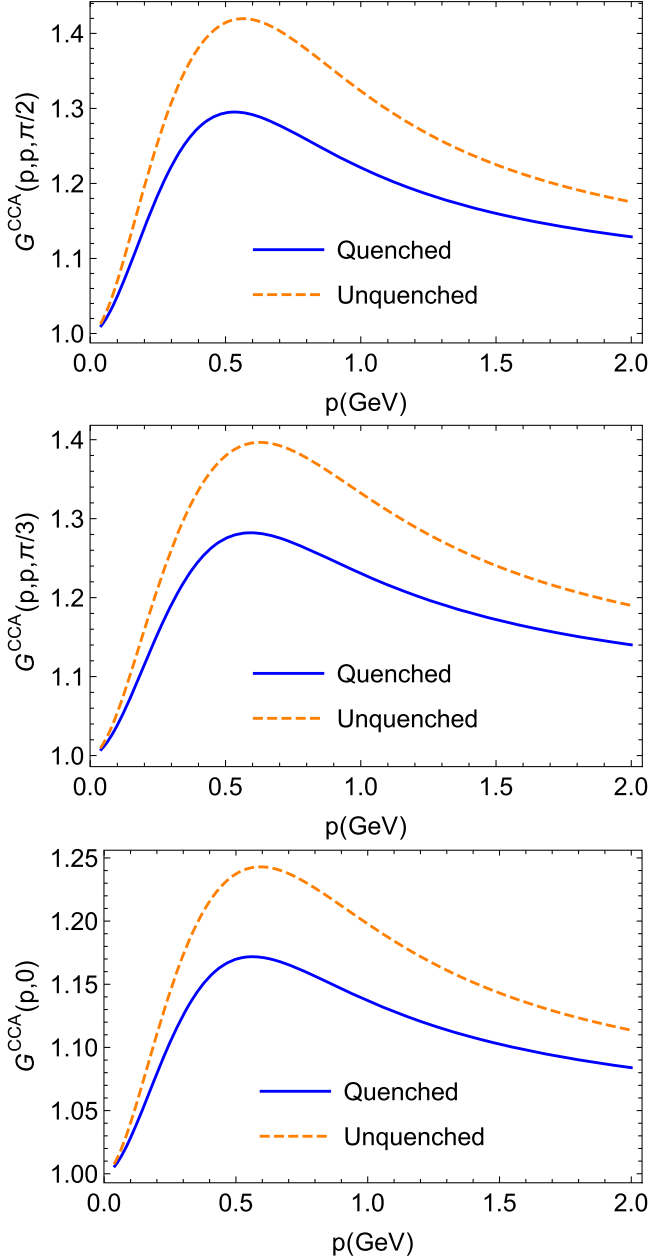


FIG. 7. Comparison of the ghost-gluon vertex in the quenched and unquenched case using the set of parameters of Table I in the orthogonal configuration (top), symmetric configuration (middle), and gluon vanishing momentum configuration (bottom).

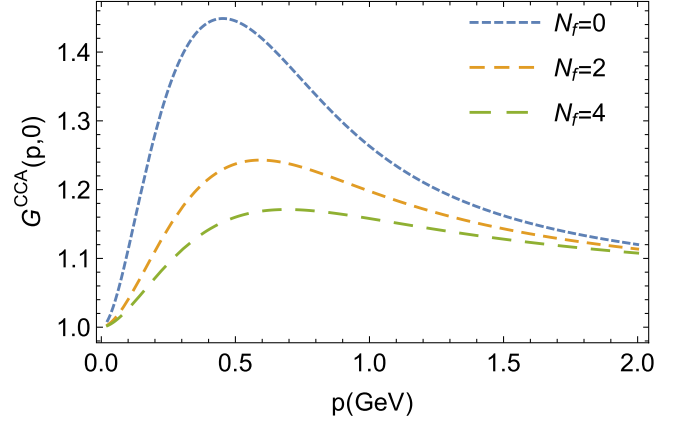


FIG. 8. Comparison of the ghost-gluon vertex when varying N_f and using the same set of parameters at 3 GeV.

where

$$\Gamma_{c^a \bar{c}^b A_\mu^c}^{(3)}(p, k, r) = -i g_0 f^{abc} \Gamma_\mu(p, k, r), \quad (26)$$

is shown in Fig. 7 for different kinematical configurations using the parameters of Table I, which are the parameters that give a better fit to one-loop propagators. It is important to mention that $G^{c\bar{c}A}(p, k, r)$ is renormalized by the combination $Z_g \sqrt{Z_A} Z_c$, which is set to one accordingly to the Taylor scheme (9). Therefore, the value of the ghost-gluon function only depends on the values of g and m for each momentum scale. In particular, the initial conditions of the renormalization flow are initialized at 1 GeV, and therefore the vertex function at that scale is purely determined by the values from Table I. As the value of g_0 is larger in the unquenched case, the unquenched vertex function will be above the quenched one, as is observed in Fig. 7.

To study the influence of dynamical quarks on the ghost-gluon vertex is therefore convenient to change the flavor number while keeping the same initial conditions of

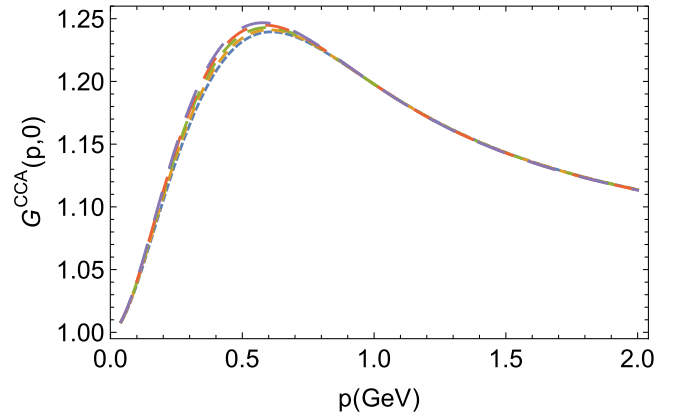


FIG. 9. Ghost-gluon vertex for different values of M_0 with fixed g_0 and m_0 .

renormalization group the flow. In Fig. 8 we compare the ghost-gluon vertex when raising N_f and using the same set of parameters at 3 GeV. It can be seen that the unquenching effects reduce the vertex contribution in the infrared. Another observation is that the unquenched ghost-gluon vertex is almost insensitive to the value of the quark mass, as is seen in Fig. 9.

VI. CONCLUSIONS

With the aim of studying the infrared properties of the gluon and ghost-gluon three-point correlation functions, we presented a one-loop calculation using the Curci-Ferrari model in Landau gauge for arbitrary kinematical configurations. The results are an extension of a previous work [53] to the unquenched case. In particular, we compared the results for the vertex with the available lattice data including dynamical quarks corresponding to the kinematical configuration with a vanishing gluon momentum and two degenerate flavors. A study of the position of the zero crossing of the vertex was also done, and we observed that the position of the zero crossing is shifted to the infrared due to the presence of dynamical quarks when compared to the quenched case.

We also studied the quenched case because some infrared properties observed by the model in the previous work were not clear in lattice simulations at that time. However, the infrared lattice study of the three-gluon vertex has

improved in the last years and now error bars are good enough to understand its infrared behavior, as discussed in Ref. [60]. In particular, lattice simulations show a change of sign in the deep infrared that is easily understood by the Curci-Ferrari model. As it has been discussed in Refs. [53,65] that this can be explained as a consequence of the diagram with a loop of massless ghosts. In the quenched case we compared the results with lattice simulations for the completely symmetric and antisymmetric configurations. The results showed an excellent match with lattice results, especially considering that the free parameters of the model were already fixed by fitting the propagators.

ACKNOWLEDGMENTS

The authors would like to acknowledge the financial support from Programa de Desarrollo de las Ciencias Básicas (PEDECIBA) and Evaluation-orientation de la COopération Scientifique (ECOS) program and from the ANII-FCE-126412 project. We also thank N. Barrios, U. Reinosa, M. Tissier, and N. Wschebor for useful discussions.

APPENDIX: CONTRIBUTION OF DYNAMICAL QUARKS

The contribution of dynamical quarks to the G_1 factor is

$$\begin{aligned} & \frac{g^2 N_f T_f}{12\pi^2 \epsilon} + \frac{g^2 N_f T_f}{12\pi^2} \left[-\frac{1}{3} + \frac{2\chi(A_0(M^2) + M^2)}{D_1} + \frac{1}{D_1 D_2} (24k^2 p^2 r^2 C_0(M^2, M^2, M^2, p, r)(S - M^2\chi) \right. \\ & \left. + \mathcal{K}_1 B_0(M^2, M^2, -p^2) + \mathcal{K}_2 B_0(M^2, M^2, -r^2) + \mathcal{K}_3 B_0(M^2, M^2, -k^2)) \right], \end{aligned} \quad (\text{A1})$$

where A_0 , B_0 , and C_0 are the corresponding finite parts of the master integrals defined in Eq. (5), and

$$\begin{aligned} \chi &= p^2 + r^2 + k^2, \\ \mathcal{S} &= p^2 r^2 + p^2 k^2 + r^2 k^2, \\ D_1 &= k^4 + p^4 + r^4 + 10\mathcal{S}, \\ D_2 &= k^4 + p^4 + r^4 - 2\mathcal{S} \end{aligned}$$

and

$$\begin{aligned} \mathcal{K}_1 &= k^6(2M^2 - p^2) + k^4(2M^2(9p^2 - r^2) - 9p^4 - 11p^2 r^2) \\ & - k^2(2M^2(9p^4 + 2p^2 r^2 + r^4) - 9p^6 + 10p^4 r^2 + 11p^2 r^4) \\ & - (2M^2 - p^2)(p^6 + 9p^4 r^2 - 9p^2 r^4 - r^6), \end{aligned}$$

while \mathcal{K}_2 and \mathcal{K}_3 are obtained by exchanging $p \leftrightarrow r$ and $p \leftrightarrow k$ in \mathcal{K}_1 , respectively.

- [1] R. Alkofer and L. von Smekal, *Phys. Rep.* **353**, 281 (2001).
- [2] L. von Smekal, R. Alkofer, and A. Hauck, *Phys. Rev. Lett.* **79**, 3591 (1997).
- [3] D. Atkinson and J. C. R. Bloch, *Mod. Phys. Lett. A* **13**, 1055 (1998).
- [4] D. Zwanziger, *Phys. Rev. D* **65**, 094039 (2002).
- [5] C. Lerche and L. von Smekal, *Phys. Rev. D* **65**, 125006 (2002).
- [6] C. S. Fischer and R. Alkofer, *Phys. Lett. B* **536**, 177 (2002).
- [7] A. Maas, J. Wambach, B. Gruter, and R. Alkofer, *Eur. Phys. J. C* **37**, 335 (2004).
- [8] P. Boucaud, T. Bruntjen, J. P. Leroy, A. Le Yaouanc, A. Y. Lokhov, J. Micheli, O. Pene, and J. Rodriguez-Quintero, *J. High Energy Phys.* **06** (2006) 001.
- [9] M. Q. Huber, R. Alkofer, C. S. Fischer, and K. Schwenzer, *Phys. Lett. B* **659**, 434 (2008).
- [10] A. C. Aguilar and J. Papavassiliou, *J. Phys. Conf. Ser.* **110**, 022040 (2008).
- [11] A. C. Aguilar, D. Binosi, and J. Papavassiliou, *Phys. Rev. D* **78**, 025010 (2008).
- [12] P. Boucaud, J. P. Leroy, A. L. Yaouanc, J. Micheli, O. Pene, and J. Rodriguez-Quintero, *J. High Energy Phys.* **06** (2008) 012.
- [13] P. Boucaud, J. P. Leroy, A. L. Yaouanc, J. Micheli, O. Pene, and J. Rodriguez-Quintero, *Few-Body Syst.* **53**, 387 (2012).
- [14] P. Dall’Olio, *J. Phys. Conf. Ser.* **378**, 012037 (2012).
- [15] M. Q. Huber, A. Maas, and L. von Smekal, *J. High Energy Phys.* **11** (2012) 035.
- [16] M. Q. Huber, *Phys. Rev. D* **93**, 085033 (2016).
- [17] J. Papavassiliou, A. C. Aguilar, D. Binosi, and C. T. Figueiredo, *EPJ Web Conf.* **164**, 03005 (2017).
- [18] M. Q. Huber, *Phys. Rev. D* **101**, 114009 (2020).
- [19] A. C. Aguilar, M. N. Ferreira, and J. Papavassiliou, *Eur. Phys. J. C* **80**, 887 (2020).
- [20] F. Gao, J. Papavassiliou, and J. M. Pawłowski, *Phys. Rev. D* **103**, 094013 (2021).
- [21] A. C. Aguilar, D. Ibáñez, and J. Papavassiliou, *Phys. Rev. D* **87**, 114020 (2013).
- [22] A. C. Aguilar, D. Binosi, and J. Papavassiliou, *Phys. Rev. D* **91**, 085014 (2015).
- [23] U. Ellwanger, M. Hirsch, and A. Weber, *Eur. Phys. J. C* **1**, 563 (1998).
- [24] J. M. Pawłowski, D. F. Litim, S. Nedelko, and L. von Smekal, *Phys. Rev. Lett.* **93**, 152002 (2004).
- [25] C. S. Fischer and H. Gies, *J. High Energy Phys.* **10** (2004) 048.
- [26] C. S. Fischer and J. M. Pawłowski, *Phys. Rev. D* **75**, 025012 (2007).
- [27] C. S. Fischer, A. Maas, and J. M. Pawłowski, *Ann. Phys. (Amsterdam)* **324**, 2408 (2009).
- [28] A. K. Cyrol, L. Fister, M. Mitter, J. M. Pawłowski, and N. Strodthoff, *Phys. Rev. D* **94**, 054005 (2016).
- [29] N. Dupuis, L. Canet, A. Eichhorn, W. Metzner, J. M. Pawłowski, M. Tissier, and N. Wschebor, *Phys. Rep.* **910**, 1 (2021).
- [30] W. Schleifenbaum, M. Leder, and H. Reinhardt, *Phys. Rev. D* **73**, 125019 (2006).
- [31] V. N. Gribov, *Nucl. Phys.* **B139**, 1 (1978).
- [32] D. Zwanziger, *Nucl. Phys.* **B323**, 513 (1989).
- [33] N. Vandersickel and D. Zwanziger, *Phys. Rep.* **520**, 175 (2012).
- [34] D. Dudal, J. A. Gracey, S. P. Sorella, N. Vandersickel, and H. Verschelde, *Phys. Rev. D* **78**, 065047 (2008).
- [35] A. Cucchieri and T. Mendes, *Phys. Rev. Lett.* **100**, 241601 (2008).
- [36] I. L. Bogolubsky, E. M. Ilgenfritz, M. Muller-Preussker, and A. Sternbeck, *Phys. Lett. B* **676**, 69 (2009).
- [37] V. G. Bornyakov, V. K. Mitrushkin, and M. Muller-Preussker, *Phys. Rev. D* **81**, 054503 (2010).
- [38] T. Iritani, H. Suganuma, and H. Iida, *Phys. Rev. D* **80**, 114505 (2009).
- [39] A. Maas, *Phys. Rep.* **524**, 203 (2013).
- [40] O. Oliveira and P. J. Silva, *Phys. Rev. D* **86**, 114513 (2012).
- [41] P. Boucaud, F. De Soto, K. Raya, J. Rodríguez-Quintero, and S. Zafeiropoulos, *Phys. Rev. D* **98**, 114515 (2018).
- [42] S. Zafeiropoulos, P. Boucaud, F. De Soto, J. Rodríguez-Quintero, and J. Segovia, *Phys. Rev. Lett.* **122**, 162002 (2019).
- [43] M. Tissier and N. Wschebor, *Phys. Rev. D* **82**, 101701 (2010).
- [44] M. Tissier and N. Wschebor, *Phys. Rev. D* **84**, 045018 (2011).
- [45] G. Curci and R. Ferrari, *Nuovo Cimento A* **32**, 151 (1976).
- [46] F. Siringo, *Nucl. Phys.* **B907**, 572 (2016).
- [47] F. Siringo, *Phys. Rev. D* **94**, 114036 (2016).
- [48] F. Siringo and G. Comitini, *Phys. Rev. D* **98**, 034023 (2018).
- [49] G. Comitini and F. Siringo, *Phys. Rev. D* **102**, 094002 (2020).
- [50] M. Peláez, U. Reinosa, J. Serreau, M. Tissier, and N. Wschebor, *Phys. Rev. D* **96**, 114011 (2017).
- [51] M. Peláez, U. Reinosa, J. Serreau, M. Tissier, and N. Wschebor, *Phys. Rev. D* **103**, 094035 (2021).
- [52] M. Peláez, U. Reinosa, J. Serreau, M. Tissier, and N. Wschebor, *Rep. Prog. Phys.* **84**, 124202 (2021).
- [53] M. Peláez, M. Tissier, and N. Wschebor, *Phys. Rev. D* **88**, 125003 (2013).
- [54] M. Peláez, M. Tissier, and N. Wschebor, *Phys. Rev. D* **90**, 065031 (2014).
- [55] M. Peláez, M. Tissier, and N. Wschebor, *Phys. Rev. D* **92**, 045012 (2015).
- [56] U. Reinosa, J. Serreau, M. Tissier, and N. Wschebor, *Phys. Rev. D* **96**, 014005 (2017).
- [57] J. A. Gracey, M. Peláez, U. Reinosa, and M. Tissier, *Phys. Rev. D* **100**, 034023 (2019).
- [58] N. Barrios, J. A. Gracey, M. Peláez, and U. Reinosa, *Phys. Rev. D* **104**, 094019 (2021).
- [59] N. Barrios, M. Peláez, U. Reinosa, and N. Wschebor, *Phys. Rev. D* **102**, 114016 (2020).
- [60] A. C. Aguilar, F. De Soto, M. N. Ferreira, J. Papavassiliou, and J. Rodríguez-Quintero, *Phys. Lett. B* **818**, 136352 (2021).
- [61] R. Alkofer, C. S. Fischer, and F. J. Llanes-Estrada, *Phys. Lett. B* **611**, 279 (2005); **670**, 460(E) (2009).
- [62] M. Mitter, J. M. Pawłowski, and N. Strodthoff, *Phys. Rev. D* **91**, 054035 (2015).
- [63] A. Cucchieri, A. Maas, and T. Mendes, *Phys. Rev. D* **74**, 014503 (2006).
- [64] A. Cucchieri, A. Maas, and T. Mendes, *Phys. Rev. D* **77**, 094510 (2008).
- [65] A. C. Aguilar, D. Binosi, D. Ibáñez, and J. Papavassiliou, *Phys. Rev. D* **89**, 085008 (2014).

- [66] A. Blum, M. Q. Huber, M. Mitter, and L. von Smekal, *Phys. Rev. D* **89**, 061703 (2014).
- [67] G. Eichmann, R. Williams, R. Alkofer, and M. Vujanovic, *Phys. Rev. D* **89**, 105014 (2014).
- [68] R. Williams, C. S. Fischer, and W. Heupel, *Phys. Rev. D* **93**, 034026 (2016).
- [69] A. L. Blum, R. Alkofer, M. Q. Huber, and A. Windisch, *EPJ Web Conf.* **137**, 03001 (2017).
- [70] A. L. Blum, R. Alkofer, M. Q. Huber, and A. Windisch, *Acta Phys. Pol. B Proc. Suppl.* **8**, 321 (2015).
- [71] A. Athenodorou, D. Binosi, P. Boucaud, F. De Soto, J. Papavassiliou, J. Rodríguez-Quintero, and S. Zafeiropoulos, *Phys. Lett. B* **761**, 444 (2016).
- [72] A. G. Duarte, O. Oliveira, and P. J. Silva, *Phys. Rev. D* **94**, 074502 (2016).
- [73] P. Boucaud, F. De Soto, J. Rodríguez-Quintero, and S. Zafeiropoulos, *Phys. Rev. D* **95**, 114503 (2017).
- [74] A. C. Aguilar, M. N. Ferreira, C. T. Figueiredo, and J. Papavassiliou, *Phys. Rev. D* **99**, 094010 (2019).
- [75] A. C. Aguilar, F. De Soto, M. N. Ferreira, J. Papavassiliou, J. Rodríguez-Quintero, and S. Zafeiropoulos, *Eur. Phys. J. C* **80**, 154 (2020).
- [76] A. C. Aguilar, M. N. Ferreira, C. T. Figueiredo, and J. Papavassiliou, *Phys. Rev. D* **100**, 094039 (2019).
- [77] E. V. Souza, M. Narciso Ferreira, A. C. Aguilar, J. Papavassiliou, C. D. Roberts, and S. S. Xu, *Eur. Phys. J. A* **56**, 25 (2020).
- [78] D. Binosi and J. Papavassiliou, *Phys. Rev. D* **97**, 054029 (2018).
- [79] L. Corell, A. K. Cyrol, M. Mitter, J. M. Pawłowski, and N. Strodthoff, *SciPost Phys.* **5**, 066 (2018).
- [80] M. Vujanovic and T. Mendes, *Phys. Rev. D* **99**, 034501 (2019).
- [81] A. Sternbeck, P. H. Balduf, A. Kızılersu, O. Oliveira, P. J. Silva, J. I. Skullerud, and A. G. Williams, *Proc. Sci. LATTICE2016* (2017) 349.
- [82] J. de Boer, K. Skenderis, P. van Nieuwenhuizen, and A. Waldron, *Phys. Lett. B* **367**, 175 (1996).
- [83] A. Weber and P. Dall'Olio, *EPJ Web Conf.* **80**, 00016 (2014).
- [84] J. Serreau and U. Reinosa, *EPJ Web Conf.* **137**, 07024 (2017).
- [85] J. Maelger, U. Reinosa, and J. Serreau, *Phys. Rev. D* **97**, 074027 (2018).
- [86] J. Maelger, U. Reinosa, and J. Serreau, *Phys. Rev. D* **98**, 094020 (2018).
- [87] N. V. Smolyakov, *Theor. Math. Phys.* **50**, 225 (1982).
- [88] A. I. Davydychev, P. Osland, and L. Saks, *J. High Energy Phys.* **08** (2001) 050.
- [89] J. S. Ball and T.-W. Chiu, *Phys. Rev. D* **22**, 2550 (1980).
- [90] S. P. Martin and D. G. Robertson, *Comput. Phys. Commun.* **174**, 133 (2006).
- [91] A. V. Smirnov, *J. High Energy Phys.* **10** (2008) 107.
- [92] D. Dudal, H. Verschelde, V. E. R. Lemes, M. S. Sarandy, R. Sobreiro, S. P. Sorella, M. Picariello, and J. A. Gracey, *Phys. Lett. B* **569**, 57 (2003).
- [93] N. Wschebor, *Int. J. Mod. Phys. A* **23**, 2961 (2008).
- [94] M. Tissier and N. Wschebor, *Phys. Rev. D* **79**, 065008 (2009).
- [95] J. A. Gracey, *Phys. Lett. B* **552**, 101 (2003).